Multichannel multiple scattering calculation of $L_{2,3}$-edge spectra of TiO_2 and $SrTiO_3$: Importance of multiplet coupling and band structure

Peter Krüger
ICB, UMR 5209, CNRS–Université de Bourgogne, BP 47870, 21078 Dijon Cedex, France
(Received 24 September 2009; revised manuscript received 8 February 2010; published 24 March 2010)

We report a theoretical study on x-ray absorption spectroscopy at the Ti-$L_{2,3}$-edge of rutile and anatase TiO_2 as well as $SrTiO_3$. Using the first-principles multichannel multiple-scattering method, we obtain good agreement with experiment in all cases. We show that both multiplet-type electron correlation effects and the long-range band structure strongly influence the spectra. The differences in line shape between the three compounds are essentially a long-range effect which reflects the different crystal structures on a length scale of 1 nm.

DOI: 10.1103/PhysRevB.81.125121 PACS number(s): 78.70.Dm, 78.20.Bh

I. INTRODUCTION

X-ray absorption spectroscopy (XAS) and the closely related electron-energy-loss spectroscopy are major tools for analyzing the structural and electronic properties of matter from a local, element-specific point of view. XAS at the transition metal $L_{2,3}$-edge directly probes the empty $3d$ states which are sensitive to local symmetry, coordination, and bonding of the transition metal atoms. However, the structural information contained in the $L_{2,3}$-edge spectra is difficult to extract because predictive computational methods for $L_{2,3}$-edge spectra have been missing. Standard first-principles methods, which employ the independent particle approximation (IPA) for the calculation of XAS, yield $L_{2,3}$-edge spectra that are often in poor agreement with experiment, especially for the early $3d$ elements. This is due to the strong particle-hole configuration mixing in the XAS final state which cannot be taken account for in the IPA.[1] Quite recently, the particle-hole coupling was included in several first-principles schemes: time-dependent density-functional theory,[2] multichannel multiple scattering,[3] and the Bethe-Salpeter equation.[4] These approaches have substantially improved over the IPA for the $L_{2,3}$-edge spectra of the early $3d$ elements. However, good results have so far only been obtained for simple systems such as bulk metals and ionic compounds in high symmetry. The practically important question is whether theory can also handle complex structures with transition metal atoms at low-symmetry sites, where the structural sensitivity of the $L_{2,3}$ edge is most pronounced and the need for predictive methods is strongest.

A good test case for answering this question is titanium dioxide which is made of distorted TiO_6 octahedra in different stackings giving rise to three natural polymorphs. The $L_{2,3}$-edge spectra are routinely used as fingerprints of the polymorphs, especially for the most stable ones, rutile and anatase.[5] The spectra of TiO_2 and $SrTiO_3$ have a main four-peak structure which is common to all tetravalent Ti compounds with TiO_6 coordination [see the $SrTiO_3$ spectrum in Fig. 1(d)]. The four-peak structure can be understood in ligand field theory as a result of the twofold spin-orbit splitting of the $2p$ level (into L_3 and L_2 lines) and the twofold splitting of the $3d$ level by the octahedral ligand field into t_{2g} and e_g states. This leads to the usual labeling of peaks as L_3-t_{2g}, L_3-e_g, L_2-t_{2g}, and L_2-e_g [see Fig. 1(d)] which we also use here for simplicity. It should be kept in mind, however, that this labeling corresponds to an independent particle picture which neglects the strong configuration mixing due to particle-hole multiplet coupling. We shall discuss this issue further in the result section.

The spectrum of the cubic system $SrTiO_3$ could be well reproduced using atomic crystal field[6,7] and cluster-model calculations.[8] Compared to $SrTiO_3$, the TiO_2 spectra display some extra fine structure, in particular, the splitting of the L_3-e_g peak into an asymmetric doublet [peaks D and E in Figs. 2(e) and 2(j)]. The latter was attributed to a noncubic ligand field effect related to the distortion of the TiO_6 octahedra by de Groot *et al.*[7,9] who used the crystal-field-

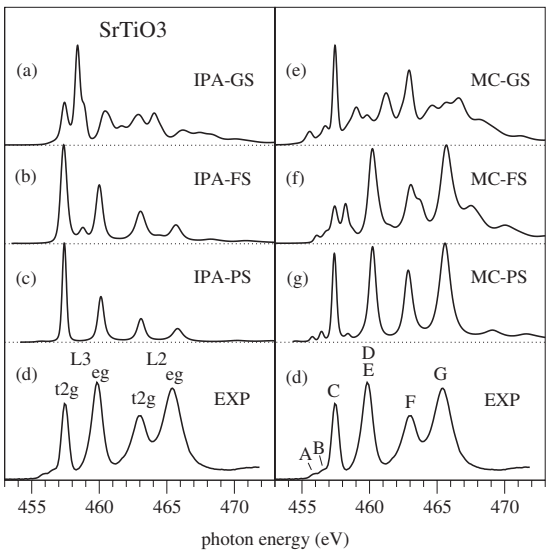

FIG. 1. Ti-$L_{2,3}$-edge spectra of $SrTiO_3$ calculated either in the IPA (left) or with the MC method including particle-hole coupling (right). GS, FS, and PS potential are compared. All spectra are normalized to equal peak height and aligned to the experimental data (EXP, taken from Ref. 12). We use two types of peak labeling for the experimental spectrum in (d). In the left panel (d) the IPA labeling is shown, which reflects only very approximately the character of the XAS final states. In right panel (d) the standard peak labeling of the TiO_2 spectra is adapted to $SrTiO_3$ for easy comparison with Figs. 2 and 3.

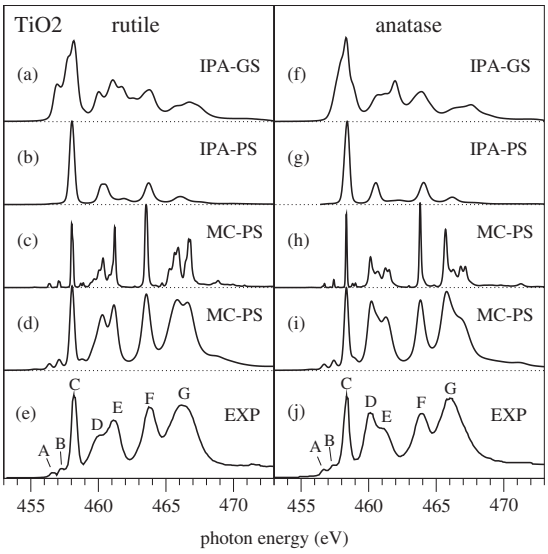

FIG. 2. $L_{2,3}$-edge spectra of TiO_2 calculated in different approximations, see legend of Fig. 1. All spectra are normalized and aligned to the EXP (taken from Ref. 17). Spectra (c) and (h) are unbroadened.

multiplet approach. This interpretation was however questioned by Crocombette and Jollet,[10] who argued that the distortion is too small to produce a sizeable splitting of the L_3-e_g peak. The rutile TiO_2 spectra has also been calculated using standard first-principles methods within the IPA.[11] While the overall $L_{2,3}$-edge line shape strongly disagrees with experiment due to the neglect of particle-hole coupling in the IPA, the D-E feature, taken alone, is well reproduced. Among the recent first-principles approaches with particle-hole coupling, the Bethe-Salpeter equation scheme was applied to $SrTiO_3$ (Ref. 12) and rutile TiO_2.[4] While good results were obtained for cubic $SrTiO_3$, the extra fine structure observed in rutile TiO_2 could not be correctly reproduced. Also time-dependent density-functional theory was applied to rutile TiO_2 but the calculated $L_{2,3}$-edge spectra were in poor agreement with experiment.[13] So despite numerous calculations in a variety of computational schemes, the $L_{2,3}$-edge spectra of TiO_2 could so far not be reproduced satisfactorily and the origin of the "fingerprint" L_3-e_g peak splitting has remained unclear.

Here we present calculations on Ti $L_{2,3}$-edge spectra using the recently developed first-principles multichannel multiple scattering (MCMS) method.[3] Very good agreement with experiment is obtained for $SrTiO_3$ and also for TiO_2 in both rutile and anatase phases. We show that the L_3-e_g peak splitting in TiO_2 is essentially a long-range effect which reflects the crystal structure on a length scale of 1 nm.

II. COMPUTATIONAL

We use the MCMS theory for $L_{2,3}$-XAS with particle-hole wave functions as developed by Krüger and Natoli.[3] This scheme features a first-principles description of the electronic structure of the extended system through the real-space multiple-scattering method and a configuration interaction calculation of the scattering matrix (T) of the absorber atom which takes full account of the energy-dependent particle-hole-multiplet coupling. The details of the method can be found in Ref. 3. Here we only describe two new features, namely, the introduction of the Fermi level and the use of LDA+U potentials.

In MCMS theory, the absorption cross section for some photon energy ω is given by

$$\sigma \propto \sum_{\alpha lm\sigma\alpha' l' m' \sigma'} M^*_{\alpha lm\sigma} \,\mathrm{Im}\, \tau^{00}_{\alpha lm\sigma,\alpha' l' m' \sigma'} M_{\alpha' l' m' \sigma'}, \quad (1)$$

where M are the matrix elements of the dipole operator and τ^{00} those of the multichannel scattering-path operator at the absorber site. α labels the quantum numbers of the photoionized system, which in the present case of a particle-hole wave function are just the quantum numbers of the $2p$ hole, i.e., (jm_j). Further lm are the orbital quantum numbers of the photoelectron and σ is its spin. τ^{00} can be calculated from

$$\tau_{\alpha\alpha'} = [T^{-1}_{\alpha\alpha'} - \delta_{\alpha\alpha'}\rho]^{-1}, \quad (2)$$

where T is the multichannel T matrix of the absorber (denoted t_0 in Ref. 3) and ρ is the reflectivity of the cluster without absorber. The site indices 00 and the quantum numbers of the photoelectron have been omitted here. Equation (2) was derived for systems with an empty d band in the ground state.[3] For the general case of partially filled and/or hybridized bands, we replace Eq. (2) by

$$\tau_{\alpha\alpha'} = [T^{-1}_{\alpha\alpha'} - \delta_{\alpha\alpha'}t^{-1} + \delta_{\alpha\alpha'}(t^{-1} - \rho)/(1-f)]^{-1}, \quad (3)$$

where t is the single particle T matrix and f the Fermi function. The quantities t^{-1}, ρ, f are evaluated at the photoelectron energy in channel α, given by $\epsilon_\alpha = \omega + E_\alpha$, where E_α is the $2p$-α level. It is easy to see that Eq. (3) reduces to the correct IPA limit in the absence of particle-hole coupling, i.e., when $T_{\alpha\alpha'} = \delta_{\alpha\alpha'}t$.

The local density approximation (LDA) systematically underestimates the band gap of insulators. The LDA band gaps as calculated with the linear muffin-tin orbital method[14] are 1.7, 1.6, and 1.4 eV in TiO_2 rutile, anatase, and $SrTiO_3$, respectively, while the experimental values are 3.05, 3.2, and 3.2 eV. We employ a simple LDA+U-type correction by shifting the self-consistent LDA potential by a constant ΔE_d for the calculation of the Ti d partial waves.[15] We take $\Delta E_d = 2$ eV for all systems which results in band gaps of 3.0 ± 0.1 eV in good agreement with experiment.

All XAS spectra [except in Fig. 3(a)] were calculated for spherical clusters of about 300 atoms and are converged in cluster size. The spectra were convoluted with a Lorentzian to account for finite core-hole lifetime and with a Gaussian of full width at half maximum (FWHM) 0.3 eV to simulate experimental broadening. Due to Coster-Kronig decay, the lifetime width of the $2p_{1/2}$ hole is much larger than that of the $2p_{3/2}$ hole. Moreover, the two core-hole states are strongly mixed in the $L_{2,3}$-XAS. In order to model lifetime broadening in this situation, we have used a Lorentzian with an energy dependent width $2\Gamma(\omega) = 0.1 + 0.072 \times (\omega - \omega_0)$ (in eV), where ω_0 is the L_3 threshold energy (after prepeaks). This is a linear interpolation between the lifetime widths

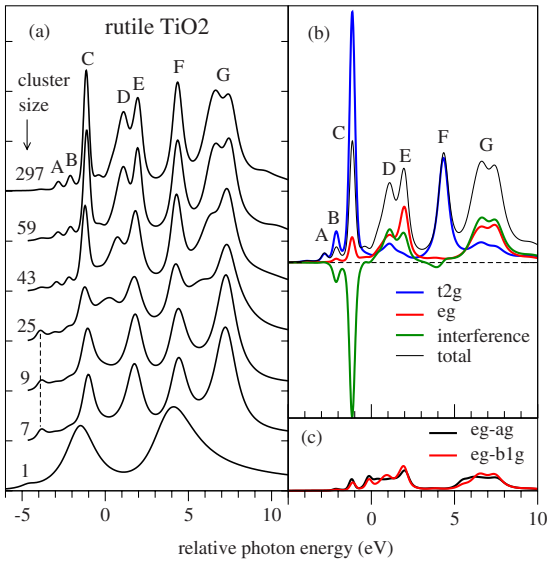

FIG. 3. (Color online) $L_{2,3}$-edge spectra of rutile TiO_2 calculated with multichannel coupling and the partially screened potential (MC-PS). (a) Spectra as a function of cluster size. (b) Projection of the 297-atom spectrum onto t_{2g}- and e_g-type d orbitals of the photoelectron. The t_{2g}-e_g interference and the sum of t_{2g}, e_g, and interference spectrum (total) are also shown. (c) Projection onto the $3z^2-r^2$ (eg-ag) and the xy orbital (eg-b1g). The same intensity scale has been used for all spectra.

reported for the $2p_{3/2}$ hole (0.1 eV) and the $2p_{1/2}$ hole (0.5 eV).[16]

III. RESULTS AND DISCUSSION

Figure 1 shows the Ti-$L_{2,3}$-edge spectra of $SrTiO_3$ calculated either in the IPA (panels a–c) or in the MC approach which includes the particle-hole configuration interaction (panels e–g). Three different one-electron potentials are compared: the ground-state (GS) potential (a,e), the full-screened (FS) core-hole potential corresponding to the final-state rule (b,f) and the partially screened (PS) potential (c,g). The final-state potential was obtained through a self-consistent calculation with a $2p$ hole at the absorber site in supercells of four formula units. The partially screened potential is the sum of $\alpha=10\%$ ground-state potential with an unscreened $2p$ hole and 90% final-state potential. This is exactly the same screening model with the same mixing value α as we have used for the Ca-$L_{2,3}$-edge spectra.[3] It can be seen from Figs. 1(a)–1(c) that the IPA yields very bad $L_{2,3}$ spectra whatever one-electron potential is used. The one-electron potential has, however, a strong effect on the line shape. In the sequence GS–FS–PS, core-hole attraction increases and thus the final-state waves become more and more localized at the absorber site. This explains the narrowing of peaks and the progessive "loss of band structure" (i.e., the loss of spectral features that are due to band formation) which is observed for the sequence GS–FS–PS in Figs. 1(a)–1(c). It can be seen that the PS potential (c) gives best agreement with experiment as far as number and positions of the peaks are concerned.

When the particle-hole coupling is taken into account through the multichannel scheme [Figs. 1(e)–1(g)], the spectra drastically change and much spectral weight is transferred from the L_3 to the L_2 edge and from the (nominal) t_{2g} peaks to the e_g peaks. The particle-hole coupling also generates new peaks, in particular, the two weak prepeaks A and B [see Fig. 1(d), right panel]. The origin of these prepeaks is well understood from atomic-multiplet calculations.[1,7] A purely atomic-multiplet calculation for a $(2p^63d^0)$ ground and a $(2p^53d^1)$ final-state configuration yields three peaks: two prominent peaks which correspond mainly to the $2p_{3/2}(L_3)$ and the $2p_{1/2}$ hole (L_2) as well as one extra and much weaker prepeak. The latter is absent in the IPA, i.e., it is a genuine multiplet effect. In an octahedral crystal field the prepeak splits into two lines,[7] which correspond to peaks A and B in Figs. 1–3. Also the multichannel spectra [Figs. 1(e)–1(g)] show a strong dependence on the one-electron potential. The partially screened potential (g) yields by far best, indeed very good agreement with experiment. This shows that the monopole term of the particle-hole interaction is incompletely screened in the $L_{2,3}$-edge spectra and that this effect can be well accounted for with the partially screened potential with $\alpha=10\%$. This fully confirms our findings obtained for Ca compounds.[3]

The Ti-$L_{2,3}$-edge spectra of TiO_2 in the rutile and anatase polymorphs are shown in Fig. 2. The comparison of the different approximations leads to the same conclusions as for $SrTiO_3$. The IPA gives wrong peak intensities for all potentials but the partially screened potential improves over the ground-state potential as far as number, width, and position of the peaks are concerned. Inclusion of the particle-hole multiplet coupling (MC-PS, panels d and i) leads to spectra in very good agreement with experiment for both rutile and anatase. In particular, the splitting of the L_3-edge peak into the two peaks D and E is well reproduced, not only for the energy splitting but also for the relative intensities of the two components D and E. The asymmetry of the D-E doublet is the fingerprint of the crystallographic phases. To the best of our knowledge, it has never been reproduced theoretically before for both rutile and anatase. The only disagreement with experiment is that in the calculated spectra (d,i), peak G has some doublet fine structure whereas a single broad peak is seen in the data. If the broadening in the high-energy part of the spectra is increased, good agreement is also obtained for peak G, as we have checked. This hints to existence of broadening mechanisms that are not taken into account here, such as vibrational broadening[7] or Ti-O charge-transfer excitations.[18] In Figs. 2(c) and 2(h) "unbroadened" MC-PS spectra are shown, where only a soft Gaussian broadening (FWHM=0.1 eV) has been applied for graphical reasons. In these spectra, peak broadening (above 0.1 eV) is intrinsic to the electronic structure of the XAS final state, namely, it is due to band formation. As will be shown in Fig. 3 below, peaks C and F correspond mainly to transitions into t_{2g} orbitals. Peaks C and F are very sharp in Figs. 2(c) and 2(h) while the features D, E, and G, which correspond mainly to transitions into e_g orbitals, are much broader. So we see that the broadening of the e_g peaks is partly due to band formation while that of t_{2g} peaks is entirely due to the core-hole decay. Note that the absence of band broadening of the t_{2g}

peaks is an excitonic, i.e., a genuine final-state effect. In the ground state, the t_{2g} states form a 2–3-eV-wide band as can be seen from the IPA-GS calculations (a,f). For the more strongly hybridized e_g orbitals the excitonic effect is much weaker and some band broadening survives in the final state.

Origin of the L_3-e_g splitting.

As mentioned in the introduction, the fingerprint L_3-e_g peak splitting in TiO_2 [peaks D and E in Figs. 2(e) and 2(j)] was first attributed to a noncubic ligand field effect due to the distortion of the TiO_6 octahedra.[7,9] Although this explanation was strongly debated in the following,[10] the ligand field scenario is still often used in the interpretation of the experimental data, probably because of a lack of convincing alternative explanations. Standard band-structure calculations in the IPA without core-hole (which correspond to our IPA-GS approximation) give a D-E feature for rutile TiO_2 which agrees quite well with experiment.[11] However, such calculations lack the prepeak structure (A and B in Fig. 2) and give intensities ratios between the four main peaks (C:D+E:F:G) close to statistical branching ratio of L_3-t_{2g}:L_3-e_g:L_2-t_{2g}:L_2-e_g which is 6:4:3:2, see Fig. 2(a). This is completely off the experimentally observed intensity ratios of about 1:2:1:2 [see Figs. 2(e) and 2(j)] and so the overall line shape obtained in standard band-structure calculations is in gross disagreement with experiment. Therefore it can be said that the origin of the characteristic L_3-e_g (or D-E) peak splitting in TiO_2 is not well understood to date.

We shall now show that the L_3-e_g peak splitting is essentially a nonlocal effect caused by long-range bonding (band-structure) properties while the local distortion of the TiO_6 octahedra plays a much smaller role. Figure 3(a) shows the $L_{2,3}$ spectra for rutile TiO_2 as a function of cluster size. Spherical clusters with open-boundary conditions were used.[19] When comparing the spectrum of a single Ti atom in Fig. 3(a) with that of the seven-atom (TiO_6) cluster, it is seen that hybridization with the first-shell O ligands produces the typical octahedral ligand field splitting[7] and leads to a four-peak structure similar to the $SrTiO_3$ spectrum [see Fig. 1(d)]. However, the characteristic (D-E) splitting of the L_3-e_g peak is missing in the calculation with the seven-atom rutile cluster. We have found the same qualitative result for a TiO_6 cluster with anatase structure (not shown). This result confirms the model calculations by Crocombette and Jollet,[10] who found that the D-E splitting is absent for TiO_6 clusters with exact atomic positions of TiO_2 rutile or anatase. The nine-atom cluster includes the second-neighbor shell which consists of two Ti atoms at about 3 Å from the absorber. This spectrum is nearly identical to that of the seven-atom cluster and it has no D-E splitting either. The 25-atom cluster has an extra peak between L_3-t_{2g} and L_3-e_g but its position does not fit the experimental peak D. It can be seen that the spectra converge for cluster sizes of about 60 atoms, which corresponds to a diameter of 1.1 nm. Only for such large clusters the D-E splitting agrees with experiment. This analysis shows that the D-E splitting is a nonlocal effect which reflects the electronic structure of the system on a length scale of 1 nm.

In order to better understand the crystal-field effects, we shall now make a decomposition of the absorption spectrum of rutile TiO_2 with respect to the orbital symmetry of the excited electron. The sums over (ll') in Eq. (1) can be restricted to d orbitals since only $p \rightarrow d$ transitions have non-negligible radial dipole-matrix elements in the case of $L_{2,3}$-edge spectra.[3] By selecting $l=l'=2$ and not summing over mm' in Eq. (1) we define a d-orbital projection matrix of the absorption cross section as

$$\sigma_{mm'}^{(l=2)} \propto \sum_{\alpha\sigma,\alpha'\sigma'} M_{\alpha 2m\sigma}^{*} \,\mathrm{Im}\, \tau_{\alpha 2m\sigma,\alpha' 2m'\sigma'}^{00} M_{\alpha' 2m'\sigma'}.$$

In rutile TiO_2 the point symmetry at the Ti sites is D_{2h}. We choose a coordinate system centered on a Ti site with oxygen ligands at $(0,0,\pm 1.983)$ and at $(\pm 1.479, \pm 1.265, 0)$ (in Å). We use real cubic d orbitals, which transform as the following irreducible representations of D_{2h}: $3z^2-r^2$ and x^2-y^2: a_g, xy: b_{1g}, xz: b_{2g}, yz: b_{3g}. In the approximate O_h symmetry, $3z^2-r^2$ and xy transform as e_g, while xz, yz, and x^2-y^2 transform as t_{2g}. We define the partial-absorption cross section for an orbital symmetry Γ as

$$\sigma_{\Gamma} = \sum_{mm' \in \Gamma} \sigma_{mm'}^{(l=2)}.$$

First we analyze the spectrum according to the approximate O_h symmetry, i.e., we project onto $\Gamma = t_{2g}, e_g$. The partial-absorption spectra for these two symmetries are shown in Fig. 3(b). The t_{2g}-e_g interference term is also shown. It was calculated as

$$\sum_{m \in t2g, m' \in eg} (\sigma_{mm'}^{(l=2)} + \sigma_{m'm}^{(l=2)}).$$

Note that the sum of t_{2g}, e_g, and interference spectrum ["total" in Fig. 3(b)] yields the full spectrum [top curve in Fig. 3(a)] as it has to be. It can be seen that peaks C and F correspond dominantly to t_{2g} orbitals and D, E, and G dominantly to e_g orbitals, in accordance with the usual labeling of peaks. However, only for peak F the photoelectron orbital character is nearly pure (t_{2g}). All other peaks show substantial orbital mixing which is seen most directly by looking at the interference spectrum. This strong interference is not due to the fact that the symmetry is lower than O_h but it is a correlation effect due to the particle-hole multiplet coupling. When the particle-hole coupling is switched off, i.e., in the IPA limit then the interference term vanishes as we have checked. In Fig. 3(c), we show the partial-absorption spectra for the orbitals $3z^2-r^2$ (denoted eg-ag) and xy (denoted eg-b1g). These orbitals transform both as e_g in O_h but they split respectively into a_g and b_{1g} in the exact D_{2h} group. It can be seen that these two partial spectra are very similar and that they cover both D and E peaks. This shows that the noncubic crystal field is weak and that it cannot explain the D-E splitting.

Next we have studied the effect of the distortion of the TiO_6 octahedra. In Fig. 4, (upper panel) we compare the TiO_2 spectrum of the real rutile structure, with that of an "ideal" rutile structure which is made of undistorted TiO_6 octahedra with the same stacking and cell volume as the real

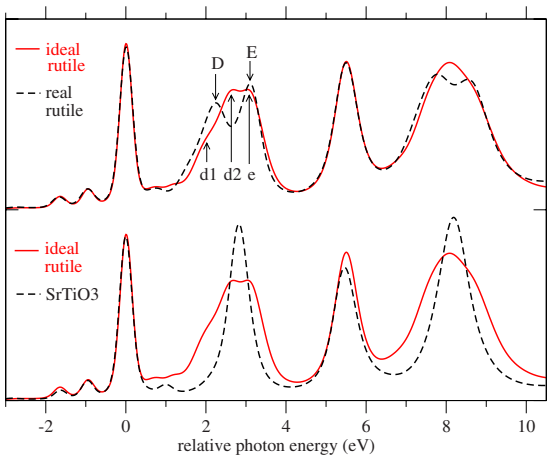

FIG. 4. (Color online) $L_{2,3}$-edge spectra calculated with MC-PS with clusters of about 300 atoms. Comparison between $SrTiO_3$ and rutile TiO_2 with either the real structure or an ideal rutile structure made of undistorted TiO_6 octahedra.

structure. In ideal rutile, the L_3-e_g peak is split into three lines (labeled d1,d2, and e) rather than into two (D,E) as in real rutile. The total width and the asymmetry of the L_3-e_g peak are however very close in the two systems. This shows that the distortion of the TiO_6 octahedra is not a necessary condition for the L_3-e_g peak splitting but the distortion is required for a clear doublet line shape. In the lower panel of Fig. 4 the ideal rutile spectrum is compared with the $SrTiO_3$ spectrum. The individual TiO_6 octahedra in these two structures are almost identical, namely, perfect octahedra with a Ti-O bond length that differs by less than 1%. So on the basis of a TiO_6 cluster model, one would expect the $SrTiO_3$ and the ideal rutile spectra to be identical. However, it is seen that the spectrum of ideal rutile differs more strongly from $SrTiO_3$ than from real rutile. We conclude that the difference in line shape between $SrTiO_3$ and rutile TiO_2 should be attributed mainly to the structural differences beyond the first nearest-neighbor shell, i.e., to the different stacking of the TiO_6 octahedra rather than to the distortion of the individual octahedra.

We may draw the following conclusions from this analysis. (a) The distortion of the TiO_6 octahedra is not a sufficient condition for the L_3-e_g peak splitting since there is no splitting for an isolated (distorted) TiO_6 octahedron. (b) The distortion is not even a necessary condition since ideal rutile made from undistorted octahedra also shows a L_3-e_g peak splitting of about the same width as real rutile. (c) The distortion has, however, a non-negligible influence on the fine structure of the L_3-e_g peak and line shapes in good agreement with experiment require big clusters with the correct stacking and distortion of TiO_6 octahedra.

IV. CONCLUDING REMARKS

In summary we have calculated the $L_{2,3}$-edge spectra of $SrTiO_3$ and TiO_2 using the multichannel multiple-scattering approach and found very good agreement with experiment. Both local multiplet and long-range band-structure interactions are necessary ingredients for a correct description of the TiO_2 spectra. We have shown that the characteristic L_3-e_g peak splitting in TiO_2 is a long-range band-structure effect which reflects the crystal structure of TiO_2 on a length scale of about 1 nm. While the distortion of the TiO_6 octahedra plays a non-negligible role for the precise shape of the L_3-e_g feature, it is neither sufficient nor necessary for producing a L_3-e_g peak splitting of the observed width. This clarification of the origin of the spectral fine structure should be helpful for a correct interpretation of $L_{2,3}$-edge spectra in nanostructured TiO_2. More generally we have shown that the multichannel multiple-scattering method provides an accurate theoretical scheme which makes it possible to account for the structural sensitivity of $L_{2,3}$-edge spectra in a predictive way.

[1] J. Zaanen, G. A. Sawatzky, J. Fink, W. Speier, and J. C. Fuggle, Phys. Rev. B **32**, 4905 (1985).
[2] J. Schwitalla and H. Ebert, Phys. Rev. Lett. **80**, 4586 (1998).
[3] P. Krüger and C. R. Natoli, Phys. Rev. B **70**, 245120 (2004).
[4] E. L. Shirley, J. Electron Spectrosc. Relat. Phenom. **144-147**, 1187 (2005).
[5] R. Brydson, H. Sauer, W. Engel, J. M. Thomas, E. Zeitler, N. Kosugi, and H. Kuroda, J. Phys.: Condens. Matter **1**, 797 (1989).
[6] G. van der Laan, Phys. Rev. B **41**, 12366 (1990).
[7] F. M. F. de Groot, J. C. Fuggle, B. T. Thole, and G. A. Sawatzky, Phys. Rev. B **41**, 928 (1990).
[8] K. Okada and A. Kotani, J. Electron Spectrosc. Relat. Phenom. **62**, 131 (1993).
[9] F. M. F. de Groot, M. O. Figueiredo, M. J. Basto, M. Abbate, H. Petersen, and J. C. Fuggle, Phys. Chem. Miner. **19**, 140 (1992).
[10] J. P. Crocombette and F. Jollet, J. Phys.: Condens. Matter **6**, 10811 (1994).
[11] M. Mattesini, J. S. de Almeida, L. Dubrovinsky, N. Dubrovinskaia, B. Johansson, and R. Ahuja, Phys. Rev. B **70**, 115101 (2004).
[12] J. C. Woicik, E. L. Shirley, C. S. Hellberg, K. E. Anderson, S. Sambasivan, D. A. Fischer, B. D. Chapman, E. A. Stern, P. Ryan, D. L. Ederer, and H. Li, Phys. Rev. B **75**, 140103(R) (2007).
[13] G. Fronzoni, R. De Francesco, M. Stener, and M. Causa, J. Phys. Chem. B **110**, 9899 (2006).
[14] O. K. Andersen and O. Jepsen, Phys. Rev. Lett. **53**, 2571 (1984).
[15] This is equivalent to the LDA+U method from the localized limit in absence of spin and orbital polarization, where $\Delta E_d = (5-n_d)(U-J)/10$ with n_d being the ground-state d-electron number, see, e.g., M. T. Czyzyk and G. A. Sawatzky, Phys. Rev. B **49**, 14211 (1994).
[16] R. Nyholm, N. Martensson, A. Lebugle, and U. Axelsson, J. Phys. F: Met. Phys. **11**, 1727 (1981).

[17] S. O. Kucheyev, T. van Buuren, T. F. Baumann, J. H. Satcher, Jr., T. M. Willey, R. W. Meulenberg, T. E. Felter, J. F. Poco, S. A. Gammon, and L. J. Terminello, Phys. Rev. B **69**, 245102 (2004).

[18] H. Ikeno, M. Frank, F. de Groot, E. Stavitski, and I. Tanaka, J. Phys.: Condens. Matter **21**, 104208 (2009).

[19] Open-boundary conditions in the multiple-scattering calculation correspond to an embedding of the cluster into a background of free electron states. For very small cluster sizes, the coupling to the free electron states leads to an extra broadening of the spectra (especially for the single atom "1" in Fig. 3) as well as to a "metallic" peak at the Fermi cutoff (marked with a dotted line in Fig. 3). However, these finite-size effects vanish quickly with increasing cluster size.